Original Article

Journal of the European Ceramic Society Volume 38, Issue 2, February 2018, Pages 403-409

https://doi.org/10.1016/j.jeurceramsoc.2017.09.047

Tough salami-inspired C_f/ZrB_2 UHTCMCs produced by electrophoretic deposition

Pietro Galizia*, Simone Failla, Luca Zoli, Diletta Sciti

CNR-ISTEC, National Research Council of Italy - Institute of Science and Technology for Ceramics, Via Granarolo 64, I-48018 Faenza, Italy

* Corresponding author, email: pietro.galizia@istec.cnr.it, telephone: +39 0546 699777

Abstract

One of the biggest challenges of the materials science is the mutual exclusion of strength and toughness. This issue was minimized by mimicking the natural structural materials. To date, few efforts were done regarding materials that should be used in harsh environments. In this work we present novel continuous carbon fiber reinforced ultra-high-temperature ceramic matrix composites (UHTCMCs) for aerospace featuring optimized fiber/matrix interfaces and fibers distribution. The microstructures - produced by electrophoretic deposition of ZrB_2 on unidirectional carbon fibers followed by ZrB_2 infiltration and hot pressing - show a maximum flexural strength and fracture toughness of 330 MPa and 14 MPa $m^{1/2}$, respectively. Fracture surfaces are investigated to understand the mechanisms that affect strength and toughness. The EPD technique allows the achievement of a peculiar salami-inspired architecture alternating strong and weak interfaces.

Keywords: Ceramic-matrix composites (CMCs); ZrB_2; Carbon fiber; EPD; Damage tolerance;

1 Introduction

Developing both strong and tough materials is a challenge of the materials science since these properties are mutually exclusive, and are simultaneously required for almost all engineering structural materials [1]. Due to this mutual exclusion, stronger and harder materials cannot be used for safety-critical applications where catastrophic failure is unacceptable. At the state of art, the best compromises between the side properties were achieved with metallic glasses, natural and biological materials, and structural and biomimetic ceramics [1]. The above advanced materials have highly complex architectures (*e.g.* hierarchical architectures are shown by biological materials and biomimetic ceramics) where the mechanisms that enhance different properties simultaneously can originate from multiple length scales [2]. Each individual contribute results in composite properties that far exceed those of their constituents and their homogeneous mixtures [2,3]. For example, the micro-architectures of nacres – which can be considered as staggered layers of brittle bricks held together by weak and stretchy mortar – play a key role in providing toughness by various damaging processes including crack deflection, crack bridging, and debonding ahead of the crack tip [4]. The strategies in dealing with strength versus toughness conflict lead to the bioinspired ceramics with 200 MPa of strength and 30 MPa $m^{1/2}$ fracture toughness, K_{IC} [5]. The strategies are more complex in the case of the developing of materials to be used in harsh environments since the fewest number of suitable materials and the impossibility to mimic the brick-and-mortar structure of nacre. Ultra-high temperature ceramics (UHTCs) are a class of ceramic refractory materials interesting for their high melting point (>3200 °C), chemical stability and resistance to erosion and ablation. For this reason, carbides and borides, such as ZrB_2, TiB_2, HfB_2, ZrC, HfC, TaC, are potential candidates components that work in extreme environment condition; thermal protection systems, leading edges in hypersonic flights and nozzles for rockets [6-8]. Among the others, ZrB_2 has the lowest density, high strength-to-weight ratio and good oxidation resistance if combined with carbides such as B_4C, SiC or metal silicides such as $MoSi_2$ [8,9]. On the other hand, like the others

UHTCs, it is susceptible to brittle fracture (K_{IC} < 5 MPa $m^{1/2}$) and displays low thermal shock resistance. It is well known that monolithic ceramics are not toughened by promoting plasticity, but they can be toughened up to 10 MPa $m^{1/2}$ by the frictional interlocking of grains (grain bridging) during intergranular fracture [10]. Since UHTCs cannot exploit *in situ* phase transformations, glassy films, and have not any ferroic order to allow the domains switch at the coercive stress at crack tip, the main strategy to (i) enhance the intergranular fracture [11] rather than the transgranular crack propagation, and (ii) increase the tortuous crack path was the development of large elongated or plate-like grains [12]. In the last years, renewed research efforts improved the damage-tolerance of ZrB_2 by moving from ceramics to Ceramic Matrix Composites (CMCs). The first CMCs enabled a toughness increase by adding short SiC fibers [13,14], and started a novel class of materials called Ultra-High Temperature Ceramic Matrix Composites (UHTCMCs) [15]. UHTCMCs based on carbon fibers dispersed into ZrB_2 matrix, can increase the failure tolerant behavior through damage processes ahead of the crack tip, such as crack deflection mechanisms, and behind of the crack tip, such as fiber bridging and fiber pull-out. These mechanisms consume energy during the fracture process, provided that the fiber/matrix interface is well designed and the chemical reactions at the fiber/matrix interface do not degrade the reinforcement properties [1,14,16,17]. By optimizing the production process to achieve an homogeneous dispersion of the UHTC matrix into the fiber preform, a good densification level and a good fiber/matrix adhesion avoiding fiber degradation, the toughness was increased up to 10 MPa $m^{1/2}$ while keeping a flexural strength of 85 - 95 MPa [15,18]. The high amount, 65 – 70 %, of well dispersed fibers, the low crack resistance of the fiber/matrix interfaces, and the weak matrix allowed the easy fiber pull-out, delamination, fiber bridging, and hence led to a non-brittle fracture [18]. In these weak matrix composites (WMCs) the matrix is subjected to multiple cracking whilst the fibers provide strength and crack tolerance, in this way after the matrix is completely fractured by multiple microcracking, the total fracture occurs with the failure of the fibers [18]. A further development for UHTCMCs in terms of toughness can be borrowed from strategy behind the solution-polymerized acrylonitrilebutadiene-styrene (ABS): the salami-like particles [19,20]. The dispersed salami-like particles consist in polybutadiene particles (PB) grafted (-*g*-) by acrylonitrile-styrene copolymer (SAN). The PB rubber particles, in the PB-*g*-SAN binary phase system, are characterized by a strong residual stress that facilitates the crazing and shearing, reducing the stresses on the crack wake. Thus, the concept of the salami-like particles is that of increasing the extrinsic crack-tip-shielding mechanisms that act behind the crack tip to inhibit its propagation. In the UHTCMCs, the corresponding microstructural features playing a similar role can be the load-bearing fibers, having a non-uniform distribution, and being concentrated in bundles where the fiber density increases at the outer periphery. Such graded structure, similar to the fiber distribution in a bamboo structure, should also enhance the specific flexural rigidity [2]. Hence, the aimed scenario is the promoting of extensive microcracking ahead of the crack tip, primarily between the bundles (in other words, along the weak matrix), which leaves uncracked-bundle bridges (the cross section should be appear like a slice of salami). The uncracked-bundle bridges (as the crazing and shearing phenomena activated by the salami-like particles [19,20]) will act as intact regions spanning the crack wake to inhibit its progress by further microcracking inside the bundles and crack deflection along the transverse orientation to the main fracture surface. At the end of the fracture processes, the salami-inspired UHTCMCs should fail under bundle pull-out mode.

In this work, Electrophoretic Deposition (EPD) technique was implemented into the conventional process for CMCs [18] in order to obtain a salami-inspired structure of UHTCMCs based on continuous carbon fibers. Even if EPD provides extraordinary control of nano- or microstructure of single- or multi-ceramics coatings and their adhesion/robustness [21], to the best of our knowledge, no one has deposited UHTC coatings on carbon fibers by EPD. The novel UHTCMC microstructure was developed and mechanically characterized in view of the above aimed scenario.

2 Material and methods

2.1 EPD process

EPD trials were performed in plane-parallel cell geometry and cathodic modality, keeping the electrodes 9 mm apart and applying constant DC potentials. Carbon fibers, C_f (Granoc XN80-6K) were treated in a tubular furnace (Nabertherm, Germany) in order to remove the size agent, and machined as unidirectional fabrics. These C_f plates were dipped in an ethanol-based colloidal suspension at 2 wt% of commercial ZrB_2 powder (H.C. Starck, grade B, Germany), and coated by applying an electric field of 11.1 V/cm for 100 s.

2.2 Slurry preparation, infiltration, and thermal treatment

The ZrB_2 powder was mixed with 5 vol% of B_4C (H.C. Starck, Grade HS, Germany), and dispersed in aqueous solution with a polyacrylate (PEI, Sigma-Aldrich- 50% (m/v) in H_2O) by ball-milling in a polyethylene bottle with SiC balls for 3 hours. The UHTCMCs were fabricated by impregnating the coated unidirectional fabrics with the slurry, and subsequently stacking 8 layers in a unidirectional configuration. Vacuum-bagging in a furnace at 90 °C for 1 hour, was used to consolidate the green composite. Sintering was conducted in a hot uniaxial pressing at 40 MPa in low vacuum using an induction-heated graphite die of 30 x 30 mm. Cycles were carried out at 1900 °C for 10 minutes.

2.3 Microstructure and mechanical characterization

The bulk densities were measured by Archimedes' method. The microstructures were analyzed with Field-Emission Scanning Electron Microscopy (FESEM, mod. ΣigmaCarl Zeiss NTS Gmbh Öberkochen, Germany) coupled with Energy-Dispersive X-ray Spectroscopy (EDXS, mod. INCA energy 300; Oxford instruments, High Wycombe, UK). 4-pt flexural strength (σ), and flexural modulus of elasticity (E) at room temperature were measured on 25 x 2.5 x 2 mm^3 (length x width x thickness, respectively) bars, using a crosshead speed of 1 mm/min on Zwick-

Roell Z050 testing machine. Fracture toughness (K_{IC}) was evaluated by fracturing chevron notched beams (CNB) in 4-pt bending configuration. The specimens were loaded with a crosshead speed of 0.05 mm/min. The test bars (25 mm × 2 mm × 2.5 mm, length x width x thickness) were notched with a 0.1 mm-thick diamond saw, and fractured using a fully-articulated steel four-point fixture with a lower span of 20 mm and an upper span of 10 mm using a screw-driven load frame (Instron, 6025).

3. Result and discussion

3.1 EPD microstructure

The EPD technique resulted in a green ZrB_2 layer that covered the entire length of the unidirectional carbon fabrics (Fig.1 (a)). The coating was crack-free and consisted of particles smaller than 4 µm (inset in Fig.1 (a)). Through the polished cross section shown in Fig.1 (b), it can be seen that the EPD produced an external thick ZrB_2 layer of 15-20 µm where the particles were well packed to each other and well stuck to the C_f surface (inset in Fig.1(b)). The inner fibers (~40 µm far from the external layer) generally showed a discontinuous coating. Due to the high “sticking parameter” [22], particles took part in the formation of the deposit until forming a coating of about 3 µm. This thickness was measured on the isolated external fibers, such as those highlighted by the arrows in Fig.1 (b). Those can be considered as isolated fibers dipped into the bulk suspension. Hence if the span between two close fibers is smaller than 6 µm it will be closed during the EPD process by the particles that arrive from the bulk of the suspension. When all the spans (ideally) perpendicular to applied electric field are filled, and the adjacent joined fibers form a continuous wall, the particles from the bulk of suspension cannot penetrate further into the fabric and further increase the external coating which grows up to 15-20 µm. In Fig.1 (b) it can be seen that the core of the fabric is isolated from the bulk suspension after the fifth layer of C_f (statistically there is a span smaller than 6 µm between the first five layers) and the inner fibers are coated by few particles. Such stuck particles should be the starting 2 vol% of dispersed particles into the liquid media that infiltrates the unidirectional fabric before the EPD process. The external layer can be addressed as the gut of those that will be the salami: the dispersed bundles of C_f into the UHTC matrix. This external layer should give rise to a good adhesion between the C_f bundles and the ZrB_2 matrix as the covalently bonded grafted PB-*g*-SAN salami-like particles [19]. Another important feature of the coated fabric is the resulted density gradient of parallel C_f between the external and the core of the fabric. It is worth to notice that fiber density is higher at the outer periphery.

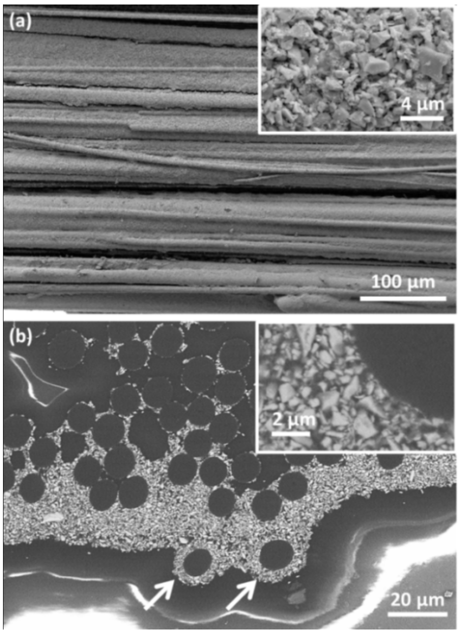

Fig.1 SEM images of dried electrophoretic deposited ZrB_2 layer on the unidirectional fabric: (a) external surface, and (b) polished cross section.

3.2 Sintered microstructure

After sintering, a fully dense microstructure was achieved (Fig.2) with a relative density of 4.1 g/cm^3. Only few triple and quadruple points between C_f were not filled during the slurry infiltration and remained after sintering, leaving 2.1 vol% of pores. The dark area within the ZrB_2 matrix (the gray area in Fig.2 (b)) are B_4C grains which are characterized by lower density, 2.5 g/cm^3, compared to the ZrB_2 (6.1 g/cm^3). The presence of B_4C particles in the ZrB_2-based slurry used to impregnate the fibers after EPD allowed us to distinguish EPD ZrB_2 from ZrB_2–B_4C matrix (see Fig. 2 b). In the sintered material, we can recognize the individual bundles circumvented by about 15 μm of EPD B_4C-free ZrB_2, immersed in the ZrB_2-B_4C matrix. Hence, the EPD favored the formation of a discrete distribution of fiber bundles inside the matrix. Furthermore it can be noticed that the C_f density is higher in the bundle periphery than in its center and, in the former, the fiber/matrix interfaces show jagged profiles (Fig.2 (c)). Since there are no evidences of interdiffusion or chemical reaction between matrix and C_f, the jagged profile should be due to the mechanical stresses that appear during the sintering process. We hypothesize that during the densification the shrinkage of ZrB_2 grains induces compressive stress into the C_f that is equilibrated by the tensile stress produced into the ZrB_2 grains around. These stresses act into concentric lines around the fiber circumference and parallel to the fiber axis, and can be released under the effect of radial shear stresses. The latter make the C_f planes slide, allowing carbon flow outward and ZrB_2 grains penetration inward. The resulting interlocking thickness (Fig.2 (b)) between ZrB_2 grains and C_f is more pronounced in the external carbon fibers layer, where the driving force for the ZrB_2 shrinkage is larger. This strong interface should guarantee the desired good adhesion between the C_f bundles and the ZrB_2 matrix.

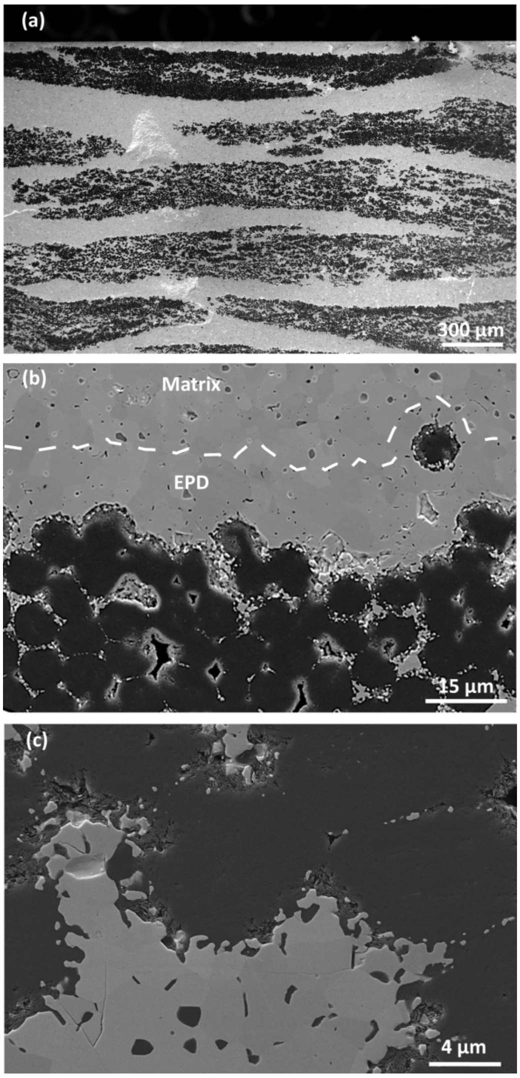

Fig.2 SEM micrograph of cross section of UHTCMC based on carbon fiber and ZrB_2/B_4C matrix.

3.3 Mechanical properties

The typical load-displacement curves are shown in Fig.3 together with the Work of Fracture (WoF) values (the area underlying the load-displacement curve divided by the doubled of the projected real surface). The average flexural strength of 284 ± 40 MPa can be ascribed to the jagged matrix/fabrics interfaces, and to higher C_f density at the outer bundles periphery. The former allows a good mechanical coupling between the matrix and the bundles, the latter allows a good stress distribution since the C_f are more concentrated where the stress is larger. These phenomena can be considered similar to what occurs in the bamboo plants where the not uniform distribution of the load-bearing fibers enables a more effective and homogeneous stress distribution [2]. It is worth to notice that the maximum flexural strength is still lower than the theoretical value of the side phases. This issue is common for the UHTCMCs and may be due to different reasons such as: tensile residual stress in the matrix due to CTE mismatch with the C_f [23,24], and no perfect alignment of the fibers. The small load drops on the load–displacement curves before the maximum flexural stress can be addressed to delaminations [25,26]. Thus, the shear or local effects which lead to delamination may be the onset cause that will leads to failure. It is likely that delamination starts inside the carbon fabric where the C_f/ZrB_2 and C_f/C_f interfaces are characterized by lower interlaminar shear strength.

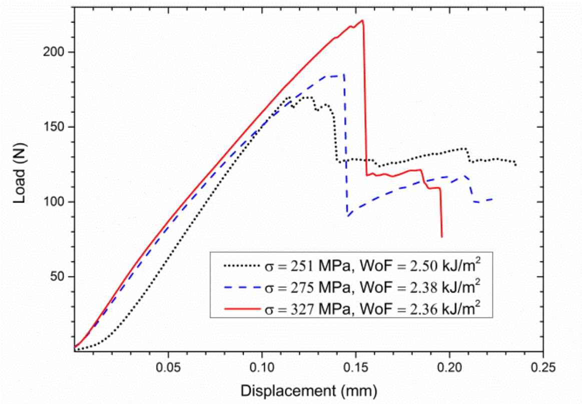

Fig.3 Load-displacement curves of 4 pt. for three different bars. The flexural strength (σ) and adsorbed energy (WoF) for each bar is reported.

In order to gain insight into the damage mechanisms occurring during flexural loading, SEM micrographs were taken after failure (Fig.4). Interfacial damage and matrix cohesive damage phenomena can be both observed. The cracks deflect inside the bundles and close to the strong matrix/C_f interface. The highly cohesive strength between fibers and matrix prevents the cracks from propagating linearly along their initial directions. The cracks turn to the adjacent layer boundary into the bundles and continue to develop. The resulting crack path is highly tortuous and formed by multiple cracks spread between the layers. This fracture development produces only partial delamination for each layer. This damage mode can sustain further loading, since the C_f inside the bundle stumps remain constrained, and should absorb more energy with consequent improvement in strength and toughness. In a similar way, the grafted PB domains cause an increase of the required fracture energy by facilitating crazing and shearing at the crack tip, and forming fibrils that act on the crack wake [19]. Hence, we think that this salami-inspired architecture on one hand allows a good stress distribution due to the C_f density gradient from inner to outer periphery of bundles. On the other side, the combination of strong (jagged) outer and (weak) inner interfaces prevents both the brittle failure of composites due to strong phases bonding and the easy interfacial debonding under low loading, in case of too weak interfaces. The fracture energy of 2.41 ±0.08 kJ/m^2 is higher than that shown by similar materials (about 0.1 kJ/m^2 [27]). The WoF decreases down to 1.4 kJ/m^2 if it is calculated from the load-displacement curves of CNB (Fig.5), due to the stress concentration at the notch. Nevertheless, this value is still one order of magnitude larger than those shown by similar materials.

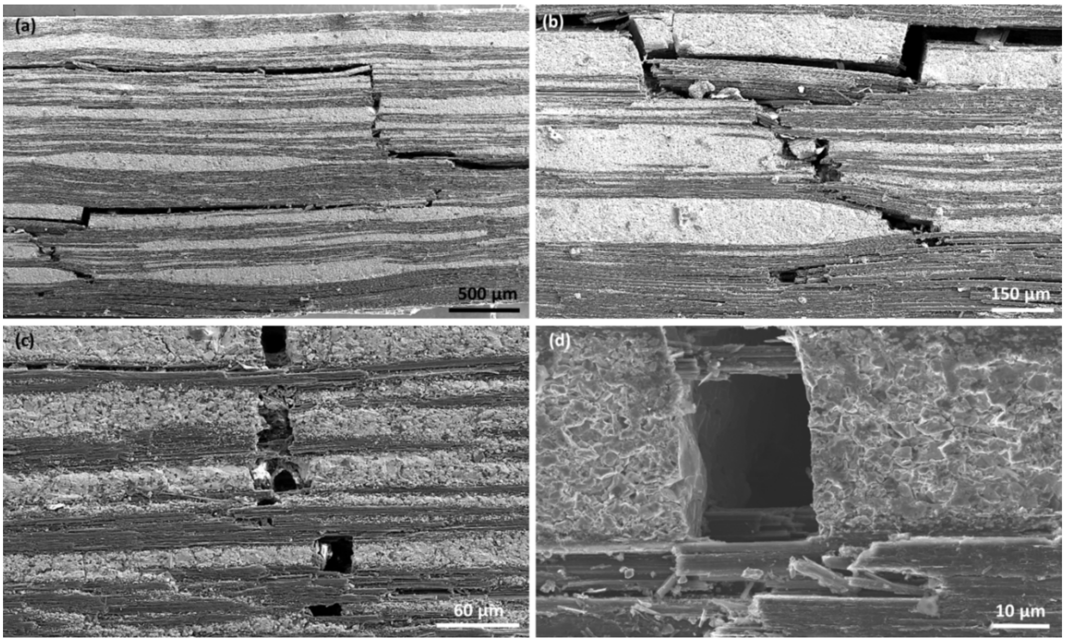

Fig.4 SEM images of failed composites under flexural loading.

The increase in fracture energy matches the increase of toughness to about 11 ± 2.5 MPa m$^{1/2}$ (Fig.5). In fact, as a general rule, cracks do not easily propagate in a material characterized by a high WoF. As seen above, the strong jagged interface between matrix and C_f acts as hindrance for the crack propagation. The crack may be stopped at that interface and activates further toughening mechanisms such as microcracking inside the bundles - where the C_f/C_f and C_f/ZrB_2 are characterized by a lower interfacial strength - and the consecutive crack deflection and propagation along the perpendicular direction. Crack deflection at the weaker interfaces is similar to what occurs in the bioinspired nacre-like composites where a weakness point is needed to fully activate the toughening mechanisms and induces the crack propagation parallel to long axis of platelet (C_f in our case) [1]. In our opinion, such an intricate microstructure gives rise to further toughening mechanisms during fracture including friction and interlocking of entire bundles of C_f, and the pull-out of single C_f from the same bundles.

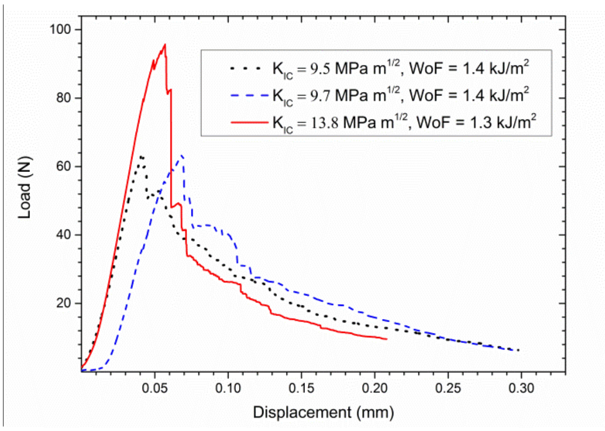

Fig.5 Load-displacement curves of 4 pt. fracture for three different chevron notched beams (CNB). The fracture toughness (K_{IC}) and adsorbed energy (WoF) for each CNB is reported.

From the fracture surface of CNB specimens that exhibit the lowest and highest fracture toughness (9.5 MPa $m^{1/2}$ (Fig.6 (a)-(c)), and 13.8 MPa $m^{1/2}$ (Fig.6 (d)-(f)), respectively), it is possible to make some qualitative considerations about the different toughening mechanisms. In both samples the matrix between the fabrics shows a brittle behaviour and the cleavage fracture is quite flat. The crack likely propagates through the matrix with a transgranular mode. In contrast, the volumetric shuffling of the material inside the fabrics is the consequence of the crack deflections. It is worth to remember that crack deflection is triggered inside the fabrics by the process zone at the crack tip. Thus the weak interfacial resistance between C_f/C_f and C_f/ZrB_2 (that characterized by a low ZrB_2/C_f ratio) inside the fabrics is necessary to take full advantage of the toughening mechanisms. The extensive delamination parallel to the C_f and the propagation of the crack mainly through the matrix leave uncracked-bundles bridges. These bridges should act as intact regions spanning the crack wake to inhibit its progress by further microcracking inside the bundles, and crack deflection along the transverse orientation to the main fracture surface. At the end of the fracture processes, the salami-inspired UHTCMCs should fail under bundle pull-out mode. Some of the footprints leaved by the pull-out of the so called salami are pointed by the white arrows in the Fig.6. In Fig.6 (f) it is clearer how their cross section appears like a slice of salami. In particular, in Fig.6 (f), it can be seen that the strong jagged interface of the fabrics is broken at the same level of the matrix, proving the good stress transmission across these strong interfaces. Moreover, it suggests that the inelastic energy dissipation through the friction interactions during the pull-out of the salami occurs at the weaker interface inside the fabrics. Based on the above discussion, it is reasonable to address the higher K_{IC} value as due to the higher amount of the footprints left from the pull-out of the salami bundles. The deep holes left by the salami pull-out can be justified by adapting the Kelly-Tyson model [28]:

$$l_c = \frac{\sigma\, r}{\tau} \tag{1}$$

where l_c is the critical length and corresponds to the lengths/depth of the fragments/hole formed after the pull-out. σ is the flexural stress of the salami (the EPD C_f fabrics), r is the equivalent radius of the projected area of the salami (the footprints leaved by its pull-out), and τ is shear stress at the weaker C_f/C_f or C_f/ZrB_2 interphases. From the Eq.1 it is clear that the pull-out of a bundle of C_f, due to the weak interphases strength (small τ) and large area (r), brings to large value of l_c, and thus dissipates a large amount of inelastic energy. On the other hand, the pull-out of the single C_f embedded in the matrix is characterized by a small l_c, about 10 μm (Fig.6

(c)). In any case, the interface debonding did not occur at the strong (jagged) interface, but inside the fiber between weakly bonded inner layers. As it can be seen in Fig.6 (e), l_c of the single pulled-out carbon fibers inside the fabrics are one order of magnitude larger than those embedded in the matrix. In fact, as said above, the interlocking thickness (*i.e.* the value of τ) between ZrB_2 grains and C_f is larger along the external matrix/fabric interface rather than ZrB_2/C_f interfaces inside the fabrics.

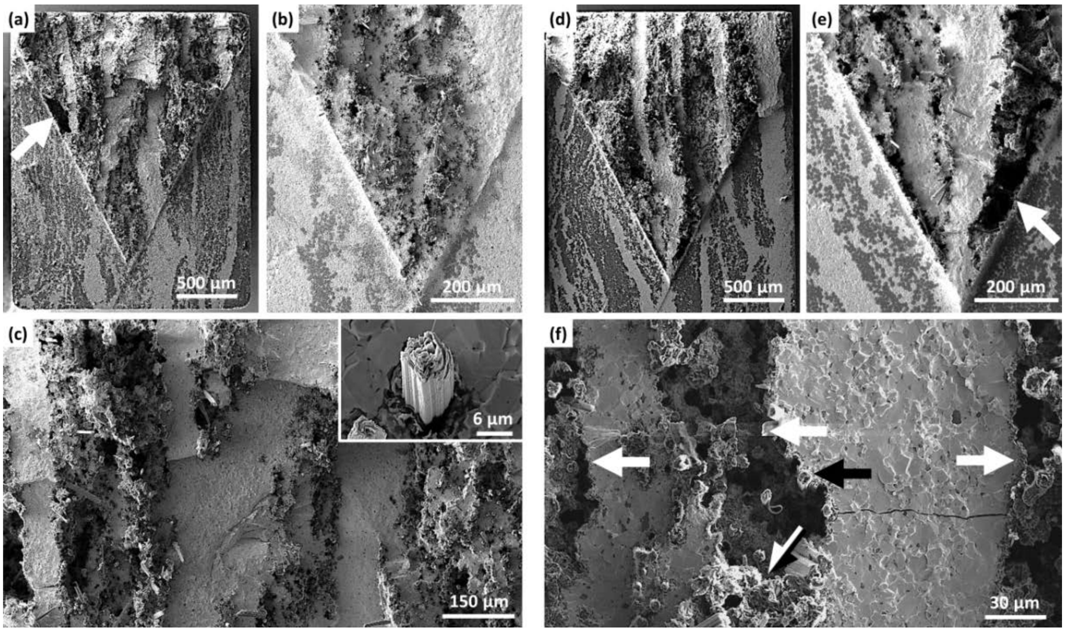

Fig.6 Transversal SEM images of failed CNB under flexural loading. (a)-(c) and (d)-(f) correspond to dotted line (K_{IC} = 9.5 MPa $m^{1/2}$) and solid line (K_{IC} = 13.8 MPa $m^{1/2}$) in Fig.5, respectively. The white arrows point some of the footprints left by the pull-out of the so called salami. The black arrow and the black and white one point a strong jagged matrix/fabric interface and a weak C_f/C_f interface, respectively.

In Fig.7 a sketch of the toughening mechanisms produced by the (a) salami-inspired C_f/ZrB_2 UHTCMCs and (b) salami-like particles is drawn. The red line represents the crack pathway. It can be seen how, for both the ceramic (Fig.7 (a)) and polymeric (Fig.7 (b)) composites, the crack tortuosity can be enhanced by microcracking and crack deflection ahead of the crack tip. For this goal, first of all, a strong mechanical coupling between the matrix and the reinforcement phase is required, as the jagged interfaces and the grafting for C_f/ZrB_2 UHTCMCs and PB-*g*-SAN, respectively. Then, the good stress distribution should allow the activation of toughening mechanisms inside the reinforcement phase, such as delamination and crazing. These crack pathways leave entire parts of the reinforcement components like the uncracked-bundle bridges for the salami-inspired composites (the cross section appears like a slice of salami), and rubber fibrils for the salami-like particles dispersed in the polystyrene matrix. These latter components give the larger extrinsic contribution that act behind the crack tip and inhibit its propagation.

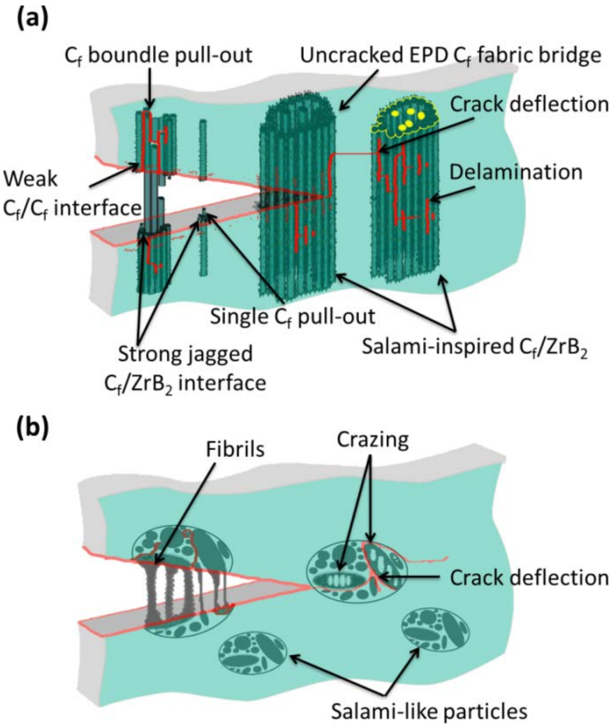

Fig.7 Sketch of the toughening mechanisms produced by the (a) salami-inspired C_f/ZrB_2 UHTCMCs and (b) salami-like particles. The red line and the yellow one represent the crack pathway and the cross section of a salami-inspired reinforcement, respectively.

The resulting damage tolerance, c, according with the Irwin equation:

$$c = \frac{K_{IC}^2}{\pi\, \sigma^2} \tag{2}$$

is 473 ±89 μm. This value is significantly higher that of the conventional ceramics of about 0.1-1 μm [29] and ZrB_2-based ceramics of about 6 μm considering typical values of strength (~800 MPa and toughness 3.5 MPa $m^{1/2}$ [6]), and approaches the lower bound of the engineering metals (Fig.8). These results suggest that salami-inspired UHTCMCs can be exploited in order to overcome the mutual exclusive properties of strength and toughness and allow to develop strong fiber reinforced ceramic composites with a high resistance catastrophic failure. Finally, although comparison with results available in the literature could be unreliable due to different preforms/matrix composition/process/measurement techniques, it is worthy to notice that our values of strength and toughness are well in agreement with those obtained for other UHTCMCs mostly obtained through enrichment of C/SiC matrix with the UHTC phase [30-32].

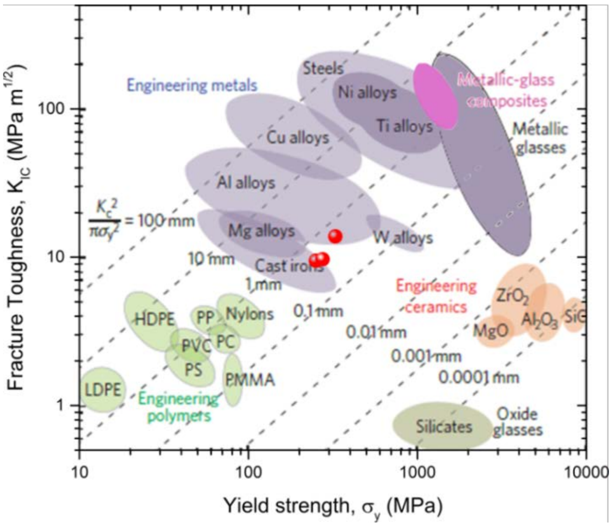

Fig.8 Data of fracture toughness (Fig.5) *vs.*flexural strength (Fig.3) plotted as red spheres on Ashby map redrawn from ref. [29]. The different levels of damage tolerance are marked with the dotted lines.

Conclusions

Ultrahigh temperature ceramic matrix composites, based on unidirectional carbon fibers dispersed in a ZrB_2 based matrix were produced by a first ZrB_2 coating of the carbon fabrics by electrophoretic deposition followed by slurry impregnation and densification at 1900 °C. The resulting microstructure consists in electrophoretic coated fabrics dispersed in a fully dense ZrB_2 matrix. The fabrics are characterized by a functionally graded concentration of fibers that is higher at the outer periphery and where the bonding of the fibers with the sintered matrix is strong. The effect of such substructures obtained by EPD was assimilated to that of the salami-like particles in the PB-*g*-SAN polymer. The salami-inspired bundles increase flexural strength (σ = 327 MPa) and enhances the extrinsic crack-tip-shielding mechanisms leading to very high fracture toughness (K_{IC} = 13.8 MPa $m^{1/2}$). The unusual combination of low density (ρ = 4.5 g/cm^3), strength and high resistance against fracture allows the production of UHTCMC with high damage tolerance (c = 570 μm) that can improve the structural component for aerospace applications. Finally, results indicate that the combination of too strong (jagged) outer interfaces and too weak (inner) interfaces can be exploited as an alternative method to achieve an overall ideal weak fiber/matrix interface.

Acknowledgements

Part of this work was funded by Ministero degli Affari Esteri e della Cooperazione Internazionale (MAECI - Italy) in the framework of Progetto di Grande Rilevanza: “ULTRAHIGH TEMPERATURE CERAMIC MATRIX COMPOSITES BY ADDITIVE MANUFACTURING USING POLYMER PRECURSORS”. This work also received support by the European Union’s Horizon 2020 research and innovation programme under Grant Agreement n°685594. (C3HARME: Next Generation Ceramic Composites for Harsh Combustion Environment and Space). C. Melandri and D. dalle Fabbriche are gratefully acknowledged for technical support.

References

[1] R.O. Ritchie, The conflicts between strength and toughness, Nat. Mater. 10 (2011) 817-

822. doi:10.1038/nmat3115.

[2] U.G.K. Wegst, H. Bai, E. Saiz, A.P. Tomsia, R.O. Ritchie, Bioinspired structural materials, Nat. Mater. 14 (2014) 23-36. doi:10.1038/nmat4089.

[3] R. Daniel, M. Meindlhumer, W. Baumegger, J. Zalesak, B. Sartory, M. Burghammer, C. Mitterer, J. Keckes, Grain boundary design of thin films: Using tilted brittle interfaces for multiple crack deflection toughening, Acta. Mater. 122 (2017) 130–137. doi:10.1016/j.actamat.2016.09.027.

[4] T.P. Niebel, F. Bouville, D. Kokkinis, A.R. Studart, Role of the polymer phase in the mechanics of nacre-like composites, J. Mech. Phys. Solids 96 (2016)133–146. doi:10.1016/j.jmps.2016.06.011.

[5] E. Munch, M.E. Launey, D.H. Alsem, E. Saiz, A.P. Tomsia, R.O. Ritchie, Tough, bio-inspired hybrid materials, Science 322 (2008) 1516–1520. doi:10.1126/science.1164865.

[6] W.G. Fahrenholtz, G.E. Hilmas, I.G. Talmy, J.A. Zaykoski, Refractory diborides of zirconium and hafnium, J. Am. Ceram. Soc. 90 (2007) 1347–1364. doi:10.1111/j.1551-2916.2007.01583.x.

[7] S.Q. Guo, Densification of ZrB_2-based composites and their mechanical and physical properties: A review, J. Eur. Ceram. Soc. 29 (2009) 995-1011. doi:10.1016/j.jeurceramsoc.2008.11.008.

[8] D. Sciti, L. Silvestroni, V. Medri, F. Monteverde, Sintering and densification mechanisms of Ultra-High Temperature Ceramics, in: W.G. Fahrenholtz, E.J. Wuchina, W.E. Lee, Y. Zhou (Eds.), Ultra-High temperature ceramics: Materials for extreme environment applications, John Wiley & Sons Inc., Hoboken, NJ, 2014, pp. 112–143. doi:10.1002/9781118700853.ch6.

[9] L. Silvestroni, G. Meriggi, D. Sciti, Oxidation behavior of ZrB_2 composites doped with various transition metal silicides, Corros. Sci. 83 (2014) 281–291. doi:10.1016/j.corsci.2014.02.026.

[10] C.J. Gilbert, J.J. Cao, L.C. Jonghe, R.O. Ritchie, Crack-growth resistance-curve behavior in silicon carbide: Small versus long cracks, J. Am. Ceram. Soc. 80 (2005) 2253–2261. doi:10.1111/j.1151-2916.1997.tb03115.x.

[11] S. Sveleba, V. Zhmurko, V. Kapustianik, I. Polovinko, Z. Trybula, Influence of electric field and mechanical stresses on the properties of incommensurate phases in $(N(CH_3)_4)_2ZnCl_4$ and $(N(CH_3)_4)_2CoCl_4$ crystals, Phys. Status Solidi 140 (1993) 573–585. doi:10.1002/pssa.2211400229.

[12] D. Sciti, S. Guicciardi, A. Bellosi, Effect of annealing treatments on microstructure and mechanical properties of liquid-phase-sintered silicon carbide, J. Eur. Ceram. Soc. 21 (2001) 621–632. doi:10.1016/S0955-2219(00)00254-5.

[13] D. Sciti, L. Pienti, A.N. Murri, E. Landi, V. Medri, L. Zoli, From random chopped to oriented continuous SiC fibers-ZrB_2 composites, Mater. Desing 63 (2014) 464-470. doi:10.1016/j.matdes.2014.06.037

[14] L. Silvestroni, D. dalle Fabbriche, C. Melandri, D. Sciti, Relationships between carbon fiber type and interfacial domain in ZrB_2-based ceramics, J. Eur. Ceram. Soc. 36 (2016) 17–24. doi:10.1016/j.jeurceramsoc.2015.09.026.

[15] L. Zoli, D. Sciti, Efficacy of a ZrB_2–SiC matrix in protecting C fibres from oxidation in novel UHTCMC materials, Mater. Design 113 (2017) 207-13. doi:10.1016/j.matdes.2016.09.104.

[16] F. Yang, X. Zhang, J. Han, S. Du, Processing and mechanical properties of short carbon fibers toughened zirconium diboride-based ceramics, Mater. Design 29 (2008) 1817-

1820. doi:10.1016/j.matdes.2008.03.011.

[17] J.J. Sha, J. Li, S.H. Wang, Y.C. Wang, Z.F. Zhang, J.X. Dai, Toughening effect of short carbon fibers in the ZrB_2 –$ZrSi_2$ ceramic composites, Mater. Design 75 (2015)160–165. doi:10.1016/j.matdes.2015.03.006.

[18] D. Sciti, A.N. Murri, V. Medri, L. Zoli, Continuous C fibre composites with a porous ZrB_2 Matrix, Mater. Design 85 (2015)127–34. doi:10.1016/j.matdes.2015.06.136.

[19] W. Heckmann, G.E. McKee, F. Ramsteiner, Structure-property relationships in rubber-modified styrenic polymers, Macromol. Symp. 214 (2004) 85–96. doi:10.1002/masy.200451007.

[20] M.M. Mazidi, M.K. Razavi Aghjeh, F. Abbasi, Fractographic analysis of the crack resistance of styrene-acrylonitrile/polybutadiene- g -styrene-acrylonitrile blends as evaluated by the essential work of fracture method, J. Appl. Polym. Sci. 131 (2014) 40072. doi:10.1002/app.40072.

[21] A.R. Boccaccini, B. Ferrari, J.H. Dickerson, C. Galassi, Special Issue: Electrophoretic deposition of ceramics, J. Eur. Ceram. Soc. 36 (2016) 263. doi:10.1016/j.jeurceramsoc.2015.08.026.

[22] B. Ferrari, R. Moreno, EPD kinetics: A review, J. Eur. Ceram. Soc. 30 (2010) 1069–1078. doi:10.1016/j.jeurceramsoc.2009.08.022.

[23] F. Monteverde, S. Guicciardi, A. Bellosi, Advances in microstructure and mechanical properties of zirconium diboride based ceramics, Mater. Sci. Eng. A. 346 (2003) 310-319.

[24] C. Praderea, C. Sauderb, Transverse and longitudinal coefficient of thermal expansion of carbon fibers at high temperatures (300–2500 K), Carbon 46 (2008) 1874-1884.

doi:10.1016/j.carbon.2008.07.035

[25] M.A. Caminero, G.P. Rodríguez, V. Muñoz, Effect of stacking sequence on Charpy impact and flexural damage behavior of composite laminates, Compos. Struct. 136 (2016) 345-357. doi:10.1016/j.compstruct.2015.10.019.

[26] S. Agrawal, K.K. Singh, P. Sarkar, Impact damage on fibre-reinforced polymer matrix composite – A review, J. Compos. Mater. 48 (2013) 317-332 doi:10.1177/0021998312472217.

[27] L. Silvestroni, D. Sciti, G.E. Hilmas, W.G. Fahrenholtz, J. Watts, Effect of a weak fiber interface coating in ZrB_2 reinforced with long SiC fibers, Mater. Desing 88 (2015) 610–618. doi:10.1016/j.matdes.2015.08.105.

[28] A. Kelly, WR. Tyson, Tensile properties of fibre-reinforced metals: Copper/tungsten and copper/molybdenum. J. Mech. Phys. Solids 13 (1965) 329–350. doi:10.1016/0022-5096(65)90035-9.

[29] M.D. Demetriou, M.E. Launey, G. Garrett, J.P. Schramm, D.C. Hofmann, W.L. Johnson, R.O. Ritchie, A damage-tolerant glass. Nat. Mater. 10 (2011) 123-128. doi:10.1038/NMAT2930.

[30] H. Hu, Q. Wang, Z. Chen, C. Zhang, Y. Zhang, J. Wang, Preparation and characterization of C/SiC-ZrB_2 composites by precursor infiltration and pyrolysis process, Ceram. Int. 36 (2010) 1011-1016. doi:10.1016/j.ceramint.2009.11.015

[31] C. Yan, R. Liu, C. Zhang, Y. Cao, Y. Wang, Effects of SiC/HfC ratios on the ablation and mechanical propeties of 3D C_f/HfC-SiC composites, J. Eur. Ceram. Soc. 37 (2017) 2343-2351. doi:10.1016/j.jeurceramsoc.2017.01.017

[32] S. Chen, C. Zhang, Y. Zhang, H. Hu, Influence of pyrocarbon amount in C/C

preform on the microstructure and properties of C/ZrC composites prepared via reactive melt infiltration, Mater. Desing 58 (2014) 570-576. doi:10.1016/j.matdes.2013.12.071